Mercury distribution in the upper troposphere and lowermost stratosphere according to measurements by the IAGOS-CARIBIC observatory, 2014-2016

Franz Slemr[1], Andreas Weigelt[2*], Ralf Ebinghaus[2], Johannes Bieser[2], Carl A.M. Brenninkmeijer[1], Armin Rauthe-Schöch[1§], Markus Hermann[3], Bengt G. Martinsson[4], Peter van Velthoven[5], Harald Bönisch[6], Marco Neumaier[6], Andreas Zahn[6], Helmut Ziereis[7]

[1]Max-Planck-Institut für Chemie (MPI), Air Chemistry Division, Hahn-Meitner-Weg 1, D-55128 Mainz, Germany

[2]Helmholtz-Zentrum Geesthacht (HZG), Institute of Coastal Research, Max-Planck-Str. 1, D-21502 Geesthacht, Germany

[3]Leibniz-Institut für Troposphärenforschung (Tropos), Permoserstr. 15, D-04318 Leipzig, Germany

[4]University of Lund, Division of Nuclear Physics, P.O. Box 118, S-22100 Lund, Sweden

[5]Royal Netherlands Meteorological Institute (KNMI), P.O.Box 201, NL-3730 AE, de Bilt, the Netherlands

[6]Institute of Meteorology and Climate Research (IMK), Karlsruhe Institute of Technology, Hermann-von-Helmholtz-Platz, D-76344 Eggenstein-Leopoldshafen

[7]Deutsches Zentrum für Luft- und Raumfahrt (DLR), Institut für Physik der Atmosphäre, D-82230 Wessling, Germany

*now with Bundesamt für Seeschifffahrt und Hydrographie (BSH), Wüstland 2, D-22589 Hamburg, Germany

[§]now with Deutscher Wetterdienst, Global Precipitation Climatology Centre, Frankfurter Straße 135, 63067 Offenbach/Main, Germany

Correspondence to: franz.slemr@mpic.de

Abstract

Mercury was measured onboard the IAGOS-CARIBIC passenger aircraft since May 2005 until February 2016 during nearly monthly sequences of mostly four intercontinental flights from Germany to destinations in North and South America, Africa, and South and East Asia. Most of these mercury data were obtained using an internal default signal integration procedure of the Tekran instrument but since April 2014 more precise and accurate data were obtained using post-flight manual integration of the instrument raw signal. In this paper we use the latter data.

Elevated upper tropospheric total mercury (TM) concentrations due to large scale biomass burning were observed in the upper troposphere (UT) at the equator and southern latitudes during the flights to Latin America and South Africa in boreal autumn (SON) and boreal winter (DJF). TM concentrations in the lowermost stratosphere (LMS) decrease with altitude above the thermal tropopause but the gradient is less steep than reported before. Seasonal variation of the vertical TM distribution in the UT and LMS is similar to that of other trace gases with surface sources and stratospheric sinks. Using speciation experiments, we show that nearly identical TM and gaseous elementary mercury (GEM) concentrations exist at and below the tropopause. Above the thermal tropopause GEM concentrations are almost always smaller than those of TM and the TM – GEM (i.e. Hg^{2+}) difference increases up to ~40% of TM at ~2 km and more above the thermal tropopause. Correlations with N_2O as a reference tracer suggest stratospheric lifetimes of 72 ± 37 and 74 ± 27 yr for TM and GEM, respectively, comparable to the stratospheric lifetime of COS. This coincidence, combined with pieces of evidence from us and other researchers, corroborates the hypothesis that Hg^{2+} formed by oxidation in the stratosphere attaches to sulfate particles formed mainly by oxidation of COS and is removed with them from the stratosphere by air mass exchange, gravitational sedimentation, and cloud scavenging processes.

1 Introduction

Mercury is an element whose high vapor pressure leads to significant emissions into the atmosphere. Measurements of atmospheric mercury show a relatively even distribution over the globe (Sprovieri et al., 2010) with concentrations varying mostly between 1 – 2 ng m^{-3} in remote areas. After oxidation to less volatile and more soluble compounds, mercury is deposited and becomes bioavailable. Its conversion to the highly neurotoxic methyl mercury which bioaccumulates in the aquatic nutritional chain to concentrations dangerous for humans and animals has motivated intensive research on the biogeochemical cycle of mercury (e.g. Mergler et al., 2007; Scheuhammer et al., 2007; Lindberg et al., 2007, AMAP/UNEP, 2013 and references therein).

Despite decades of research, the atmospheric mercury cycle is still not well understood (Lin et al., 2006; Lindberg et al., 2007, Ariya et al., 2015). Several mechanisms of elemental mercury oxidation in the gas phase have been proposed (Selin et al., 2007; Holmes et al., 2010; Dibble et al., 2012; Horowitz et al., 2017, Travnikov et al., 2017) but their relative importance is still unknown (Lin et al., 2006; Travnikov et al., 2017). Neither have the oxidation products been unequivocally identified so far because of the lack of speciation techniques for individual mercury compounds (Gustin et al., 2015; Ariya et al., 2015). In addition, attempts to constrain the atmospheric mercury cycle using different models had to rely almost exclusively on measurements at the surface in the northern hemisphere, which undermined these efforts. Measurements of mercury distribution in the troposphere and stratosphere by research aircraft are expensive and thus usually limited to short-term campaigns covering small regions of the globe (Ebinghaus and Slemr, 2000; Friedli et al., 2001, 2003a and 2004; Banic et al., 2003; Ebinghaus et al., 2007; Radke et al., 2007, Talbot et al., 2007a and b, Swartzendruber et al., 2008; Slemr et al., 2009; Lyman and Jaffe, 2012; Brooks et al., 2014, Slemr et al., 2014; Ambrose et al., 2015; Gratz et al., 2015; Weigelt et al., 2016a and b). These measurements have so far provided information about the emissions of mercury from biomass burning (Friedli et al., 2001, 2003a and b; Ebinghaus et al., 2007) and from industrial sources (Friedli et al., 2004; Talbot et al., 2007b; Swartzendruber et al., 2008, Slemr, et al., 2014; Ambrose et al., 2015; Weigelt et al., 2016b), with sometimes differing information about the vertical distribution of mercury (Ebinghaus and Slemr, 2000; Radke et al., 2007; Talbot et al., 2007a and b; Slemr et al.,

2009; Lyman and Jaffe, 2012; Brooks et al., 2014; Weigelt et al., 2016a; Bieser et al., 2017). In addition, a pronounced depletion of elemental mercury in air masses influenced by the stratosphere has been reported (Ebinghaus et al., 2007; Radke et al., 2007; Talbot et al., 2007a and b, Swartzendruber et al., 2008, Slemr et al., 2009; Lyman and Jaffe., 2012). Because of temporal and spatial limitations resulting from the costs of research aircraft hardly any information on seasonal variation of mercury concentrations in the upper troposphere (UT) and lowermost stratosphere (LMS) have been obtained so far.

IAGOS-CARIBIC (*I*n-service *A*ircraft for a *G*lobal *O*bserving *S*ystem - *C*ivil *A*ircraft for *R*egular *I*nvestigation of the Atmosphere *B*ased on an *I*nstrumented *C*ontainer) project offers a possibility of regular large scale sounding of trace gas distributions in the UT/LMS using an instrumented container flown onboard a passenger aircraft during intercontinental flights (Brenninkmeijer et al., 2007, www.caribic-atmospheric.com). From May 2005 until February 2016 mercury was measured with a modified Tekran instrument in combination with a large suite of other trace gases and particles onboard the CARIBIC aircraft (Brenninkmeijer et al., 2007, Slemr et al., 2009, 2014, 2016). The mercury data collected during nearly monthly sequences of mostly four intercontinental flights from Germany to destinations in North and South America, Africa, and East and South Asia represent the largest mercury data set obtained in the UT and LMS so far. Most mercury data were obtained using the Tekran internal default signal integration procedure but since April 2014 we manually integrated the Tekran raw signal after the flights. The post-flight integration of the raw signal substantially improved the detection limit and precision of the mercury measurements and removed negative bias of the default integration leading to occasional occurrence of zero concentrations in the data before April 2014 (Slemr et al., 2016; Ambrose, 2017). Raw signal data are available only since April 2014 and older data cannot be reintegrated. We use here the recent, smaller but higher quality dataset, in an attempt to unravel the behavior of mercury in the UT/LMS.

2 Experimental

The CARIBIC container (Brenninkmeijer et al., 2007; www.caribic-atmospheric.com) onboard an Airbus 340-600 of Lufthansa holds automated analyzers for gaseous mercury, CO, O_3, NO, NOy, CO_2, CH_4, acetone, acetonitrile, water vapor (total, gaseous, isotope composition), and fine aerosol particles (three counters for particles with lower threshold diameters of 4 nm, 12 nm, and 18 nm, upper cut off about 2.0 µm), as well as an optical particle size spectrometer (OPSS) for particles with diameters > 150 nm. In addition, whole air and aerosol particle samples are taken in flight and subsequently analyzed for greenhouse gases, halocarbons, hydrocarbons, and particle elemental composition. The CARIBIC measurement container is usually deployed monthly during a sequence of four intercontinental flights.

The air inlet system and the mercury instrument are described in detail by Brenninkmeijer et al. (2007) and Slemr et al. (2016), respectively. Briefly, the trace gas inlet consists of a trace gas diffuser tube with a flow of more than 2000 volume-l min^{-1} from which ~80 volume-l min^{-1} is taken at a right angle to a manifold which supplies the trace gas analyzers in the container via a temperature controlled PFA lined supply line. The large air velocity in the trace gas diffuser tube and perpendicular sampling at much smaller velocity discriminate against particles larger than about one micrometer diameter (~50% aspiration efficiency, Baron and Willeke, 2001). A modified Tekran instrument (Tekran-Analyzer Model 2537 A, Tekran Inc., Toronto, Canada) samples 0.5 l (STP, i.e. 1013.25 hPa and 273.15 K) min^{-1} of air from the supply line manifold (heated to 40°C) using the 4 mm ID PFA tubing at about 30°C. The major modifications of the instrument were the addition of a second pump supporting the internal Tekran pump and of a computer which communicates with the container master computer and controls the automatic operation of the instrument. For the period August 2014 until February 2016 a quartz wool scrubber was installed in the instrument to filter out gaseous oxidized mercury (GOM).

To achieve an improved spatial resolution of ~ 75 km, the instrument was run with a sampling time of only 5 min. Despite an additional pump the nominal flow of 0.5 l (STP) min^{-1} could not be sustained at the highest flight levels. Limited air flow, the short sampling time, and low concentrations resulted in only ~2 pg of mercury which is much smaller than

10 pg considered as minimum for bias-free internal default integration of the signal by the Tekran instrument (Swartzendruber et al., 2009; Slemr et al., 2016; Ambrose, 2017). The raw analyzer signals were thus processed post-flight using a manual integration procedure described in detail by Slemr et al. (2016). The detection limit and precision with post-flight processing is estimated to be ~0.05 ng m^{-3}. The instrument is calibrated after every second flight sequence by comparison with a calibrated reference Tekran instrument in the laboratory. All mercury concentrations are reported in ng Hg m^{-3}(STP).

As discussed in detail by Slemr et al. (2016) we can assume that our measurements encompass gaseous elemental mercury (GEM), gaseous oxidized mercury (GOM), and about 70% of particle bound mercury (PBM). Speciation experiments with soda lime and KCl coated quartz sand as GOM scrubbers made during several flights demonstrated that GOM passes through the CARIBIC sampling system. According to the extrapolation of the reported GOM/PBM (GOM and PBM are both assumed to be Hg^{2+}, i.e. PBM + GOM = Hg^{2+}) partitioning equilibria (Rutter and Schauer, 2007; Amos et al., 2012) from ambient temperatures near ground to about -50°C around the tropopause, most of Hg^{2+} will be attached to particles. Although the CARIBIC trace gas inlet is not optimized to collect particles, we estimated that particles with diameter of < 0.5 µm will pass through it, representing ~70% of the aerosol mass. Despite of significant PBM concentrations in the stratosphere reported by Murphy et al. (1998, 2006), we were not able to detect mercury in aerosol samples collected by the CARIBIC impactor sampler downstream of the inlet optimized for quantitative particle sampling. Although not equipped with heaters, the air carrying particles will warm up to ~ +30° on the way from the aerosol inlet to the impactor. Our inability to detect mercury in particle samples thus suggests that Hg^{2+} on particles evaporates when the air sample is heated to ~ +30°C in the inlet tubing and forms GOM. In summary, we assume that our measurements are close to total mercury (TM = GEM + Hg^{2+} = GEM + GOM + PBM) concentration and we refer to them as such.

In order to get information about the GEM fraction, sample air was passed through a quartz wool scrubber of GOM (Lyman and Jaffe, 2012) during the outbound flights between August 2014 and February 2016. The discussion of the use of scrubbers and denuders has

been going now for more than a decade, so far without any firm conclusion on a reliable and accurate method of separating GEM, GOM, and PBM (Gustin et al., 2014). As described in Supplementary Information the quartz wool scrubbers were operated within the range of parameters tested by Lyman and Jaffe (2012) and we thus expect our data to be of comparable quality to theirs. The data collected with quartz wool scrubber are referred here as GEM. However, during half of the flights with quartz wool scrubber GEM concentrations were significantly higher than those of TM during the return flight at the beginning of the flight and the difference decreased during the flights indicating contamination. We found that the contamination started to occur after the change of the personnel operating the instrument and thus attributed it to this change. These data were eliminated from the data set. We note that the tracks and altitudes of the outbound and return flights differ sometimes substantially, especially in the case of the flights to North America (the flight tracks from Germany to North America tend to be substantially further north than those of the return flights). The TM and GEM data are thus not directly comparable even if they were measured on the same day.

The data reported here were obtained during flights between April 2014 and February 2016 whose tracks are shown in Figure 1. All but one monthly flight sequences consisted of four individual intercontinental flights. The altitude of these flights varies typically from ~ 9 km at the beginning of the flight to 11 - 12 km at the end before the final descent. In addition to the meteorological data provided by the aircraft, meteorological parameters along the flight track were calculated from the ECMWF (European Centre for Medium Range Weather Forecasts) data (6-hourly, 60 model levels until February 2006 and 90 model levels thereafter, $1^{o} \times 1^{o}$ horizontal resolution). Eight days backward, 3-D kinematic trajectories were calculated with the KNMI model TRAJKS (Scheele et al., 1996, http://projects.knmi.nl/campaign_support/CARIBIC/) at one minute intervals along the flight path. Consequently, 5 trajectories were available for each mercury measurement. The data set consists of 33 and 17 individual flights with valid TM and GEM data, respectively.

For the data evaluation, the complementary continuous meteorological and chemical data were averaged over the sampling intervals of mercury measurements.

3 Results and discussion

3.1 Latitudinal TM distribution in the upper troposphere

Figure 2 shows latitudinal distribution of TM in the upper troposphere (defined as TM concentrations at potential vorticity (PV) of $-1.5 \leq PV \leq 1.5$ PVU, 1 PVU = 10^{-6} K m^2 kg^{-1} s^{-1}) observed during the flights to South America (Bogota, São Paulo, and Rio de Janeiro) in boreal summer (only July and August), fall (September, October, November), and winter (December, January, February). Corresponding latitudinal distributions of acetonitrile (AN), originating almost solely from biomass burning, and of CO and CH_4 with large emissions from biomass burning (Andreae and Merlet, 2001) are also shown. The lowest TM concentrations are observed in the latitude bands of 10 – 20°S and 20 - 30°S in summer (JA) and the same applies for CO, CH_4, and acetonitrile. The highest TM concentrations in 20-30°S latitude band are observed in fall (SON) and the TM concentrations decrease in winter (DJF) as do the CO and acetonitrile mixing ratios in the 10 – 20°S latitude band. The highest CO and CH_4 mixing ratios at 20 – 30°S are observed in winter with mixing ratios in fall somewhat lower. Biomass burning in South America starts in June, peaks in September and ends in December (Duncan et al., 2003). TM concentrations in the southernmost latitude bands follow this seasonal variability as do the acetonitrile, CO and CH_4 mixing ratios at 10 – 20°S latitude. In the latitude band 20 – 30°S the CO and CH_4 mixing ratios are higher in boreal winter than in fall. This might result from larger additional CO and CH_4 sources in boreal winter such as from oxidation of volatile organic compounds and wetlands. It is also worth noting that in boreal fall and boreal winter the acetonitrile and CO mixing ratios in the monitored part of the southern hemisphere are higher than in the northern hemisphere. In summary, Figure 2 illustrates the large-scale influence of biomass burning on the latitudinal TM distribution in the upper troposphere of the southern hemisphere.

The role of biomass burning is further illustrated by means of Figure 3, comparing the South America boreal winter profiles of the four trace constituents with those for South

Africa (Cape Town). Acetonitrile and CO mixing ratios from flights to South Africa show a pronounced bulge between 30°S and 20°N peaking around the equator. The same applies to results for the flights to South America, be it with somewhat lower values and more southern maximum for acetonitrile. For both flight routes CO and acetonitrile mixing ratios are higher in the southern than in the northern hemisphere. Boreal winter (DJF) is an intermediate season between biomass emissions peaking in September in southern Africa and in January in northern Africa (Duncan et al., 2003). The latitudinal pattern of CH_4 is less clear, with wetlands also being a major source. Finally, Figure 3 shows a similarity between TM and the biomass burning indicators in the tropics at flight altitude.

Biomass burning plumes with enhanced mercury concentrations have been reported before (Brunke et al., 2001; Friedli et al., 2001, 2003a and b, Ebinghaus et al., 2007, Slemr et al., 2014, among others). With 675 Mg yr^{-1} biomass burning is estimated to be the third largest source of atmospheric mercury after emissions from oceans (2682 Mg yr^{-1}) and from fossil-fuel power plants (810 Mg yr^{-1}; Friedli et al., 2009; Pirrone et al., 2010). Figures 2 and 3 illustrate the influence of biomass burning on the large scale distribution of TM in the southern hemispheric UT.

Acetonitrile mixing ratios in winter (DJF) in Figure 3 are the lowest in the northernmost latitude bands 20 – 50°N. The concomitant elevated TM concentrations and CO and CH_4 mixing ratios are thus mostly due to anthropogenic emissions. An exception is the highest TM concentration observed at 30 – 40°N (Figure 2) in summer (JA) which coincides with the peak of acetonitrile mixing ratio in the northern hemisphere. The respective data originate from the flight #475 from São Paulo to Munich on August 21, 2014. Two whole air samples were taken within this latitude band of which sample #12 coincides with the peak acetonitrile, acetone, CO, and CH_4 mixing ratios. In addition, sample #12 contains high ethane and propane mixing ratios (786 and 126 ppt, respectively) as well as somewhat elevated CH_4 and SF_6 mixing ratios. Sample #12 was taken over southwestern Spain and its 8 days backward trajectory crosses the Atlantic Ocean, eastern US, Great Lakes up to Californian Pacific coast. The complex composition of this sample indicates a mixture of anthropogenic pollution with emissions from biomass burning. The latter is additionally

supported by fire maps (https://lance.modaps.eosdis.nasa.gov/imagery/firemaps) reporting individual fire counts along the trajectory in North America and especially a large fire in northern California at the time of trajectory crossing.

3.2 Seasonal variation of the vertical TM distribution in the upper troposphere and lowermost stratosphere

Due to the geographical location of the airport of departure and the CARIBIC destinations it happens to be that about half of the intersected air masses are above the tropopause. This allows a fairly representative mapping of measured trace species around the tropopause. Figure 4 shows the seasonal pattern of the average TM concentrations and CO, CH_4, and O_3 mixing ratios relative to the thermal tropopause. The distance relative to the tropopause is based on CARIBIC ozone measurements. Basically, an ozone mixing ratio measured by CARIBIC is compared to representative data from ozone soundings. Because these soundings measure both thermal tropopause height and ozone, the distance relative to the tropopause is obtained (Sprung and Zahn, 2010). This value based on the CARIBIC ozone data is considered to be more accurate than PV (calculated from the ECMWF-model) based dynamical tropopause, especially in subtropical latitudes where the dynamical tropopause is not well defined by a constant PV threshold value (Kunz et al., 2011). Only measurements north of 20°N were considered for making this plot. The seasonal variation of the vertical distributions of the trace gases and TM reflect their source location and the Brewer-Dobson circulation with a maximum content of stratospheric air in the UT/LMS in spring (Holton et al., 1995; Gettelman et al., 2014). Ozone rich air, depleted in CO, CH_4, and N_2O descends in spring and the question is what happens to the mercury compounds.

The highest tropospheric TM concentrations of 1.4 – 1.7 ng m^{-3} are encountered in September/October at 0.5 – 1.75 km below the thermal tropopause. About two thirds of these elevated TM data originate from flights from Tokio to Munich on October 30, 2014, and Beijing to Munich on October 31, 2014, and were observed mostly within ~1500 km of Tokio and Beijing. High TM concentrations are accompanied by elevated CO and CH_4 mixing ratios. Near Tokio and Beijing also elevated SF_6 mixing ratios were observed.

Backward trajectories from these flight segments on October 30 and 31 point to surface contact in Tibet, Bangladesh, and northern India. Slightly elevated TM concentrations encountered near Munich on October 30 and 31 are most likely due emissions located in North America.

The lowest TM concentrations of 0.4 – 0.6 ng m^{-3} were encountered during the flights Tokio to Munich (CARIBIC #502) on April 21, 2015, and Mexico to Munich (CARIBIC #504) on April 22, 2015. During both flights the lowest TM concentrations were accompanied by O_3 and H_2O mixing ratios of > 400 ppb and < 10 ppm, respectively, characteristic of deeper stratospheric air. No CO data are available for the CARIBIC flight #502 but CO mixing ratios of < 30 ppb for the lowest TM values during the CARIBIC flight #504 also point to deep stratospheric origin of the air, as confirmed by the extremely low SF_6 and CH_4 mixing ratios in both flights.

3.3 Speciation in the UT and LMS

The reason to show only TM in Figure 4, and not GEM as well is that speciation failed for about half of the data due to contamination problems with the quartz wool GOM scrubber. For analyzing the GEM results, we divide the data set into boreal winter (December – May) and boreal summer (June – November). Figure 5 give the vertical distributions of TM and GEM in three different latitude bands for boreal winter (Figure 5a) and summer (Figure 5b). The data points in these figures represent concentration averages and their standard errors. Although extreme individual values were eliminated using the Nalimov outlier test (Kaiser and Gottschalk, 1972), unedited data give very similar plots. We also note that TM and GEM data from all flights were used in these figures, altogether 1528 and 1349 TM measurements in winter and summer, respectively, as well 699 and 916 GEM measurements in winter and summer, respectively. As already mentioned GEM data were collected during the outward and TM data during the return flights. Because of different flight tracks and flight altitudes the GEM and TM data cannot be directly compared even if measured on the same day. In addition, because of contamination problems valid GEM data are available only for about one half of the flights with TM data.

Winter vertical distribution in Figure 5a shows for 30 – 60°N a steep gradient of TM concentrations across the thermal tropopause from ~ 1.25 ng m^{-3} in the UT to ~ 0.6 ng m^{-3} in the LMS. This gradient corresponds to the steep gradient of TM concentrations in January – May shown in Figure 4. The GEM gradient is steeper starting with concentrations of ~ 1.35 ng m^{-3} and decreasing to concentrations of ~ 0.35 ng m^{-3} in the LMS. The difference between TM and GEM concentrations at altitudes starting at 1 km above the tropopause is ~ 0.2 ng m^{-3}, representing ~ 40% of TM concentration.

TM and GEM data between 30°S – 30°N cover essentially only the UT because the aircraft cruising altitude of 10 – 12 km is not sufficient to enter the tropical stratosphere. TM and GEM concentrations are essentially the same, but with ~1.2 ng m^{-3} somewhat lower than in the UT at 30 – 60°N where most of the anthropogenic mercury sources are located.

In the northernmost latitude band (> 60°N) there are few UT data because the aircraft cruising altitude of 10 – 12 km has most of the time been above the tropopause. Starting at altitudes of 1 km above the tropopause, the TM concentrations around ~ 0.6 ng m^{-3} are only slightly higher than GEM concentrations of 0.5 ng m^{-3}. Larger difference between TM and GEM concentrations is observed only at the three highest altitudes above the tropopause.

Figure 5b shows the summer data which are generally higher than the winter data. In the tropical UT (30°S – 30°N) GEM concentrations are with ~ 1.2 ng m^{-3} somewhat lower than those of TM, but the difference is probably insignificant. In the northern midlatitudes the GEM concentrations measured in the UT are higher than TM. This is not a contradiction because of the different tracks of outbound (GEM measurements) and return (TM measurements) flights to North America and different influence of biomass burning on particular flights. It appears that in the LMS the differences are small.

At mid latitudes and north of 60°N, TM gradients around the tropopause are much less steep in summer than in winter (Figure 5a), which is consistent with the seasonal variation of TM concentrations in UT/LMS shown in Figure 4. There is not much difference between

372 TM and GEM concentrations in the midlatitude LMS, but at >60°N at 2 – 3 km above the
373 tropopause GEM concentrations with ~ 0.6 ng m^{-3} are consistently lower than those of TM
374 with ~0.8 ng m^{-3}.
375
376 In summary, TM concentrations are lowest (with ~ 0.5 ng m^{-3}) in stratosphere at the highest
377 altitude above the tropopause (3 – 4 km). GEM concentrations are comparable to those of
378 TM in the UT, but systematically smaller in the LMS at middle latitude in winter and at
379 northernmost latitudes in summer.
380
381 Our notion about the behavior and speciation of mercury in the UT/LMS is quite limited
382 and based on a few measurement reports. Swartzendruber et al. (2006) observed at Mount
383 Bachelor higher GOM concentration in downslope air flow than in upslope flow which
384 implies higher GOM concentrations in the free troposphere than in the planetary boundary
385 layer. Talbot et al. (2007a) reported a total depletion of GEM in the UT/LMS. By
386 extrapolation of measurements in stratospheric intrusions, Lyman and Jaffe (2012) derived
387 an empirical model which predicts a total depletion of GEM at ~ 1 km above the tropopause
388 and of total mercury (including particle bond mercury, PBM) at some 2 km above the
389 tropopause. Brooks et al. (2014) reported decreasing GOM concentrations above GOM
390 maxima at ~ 4 km altitude above ground. They also found that GEM concentrations are
391 independent of altitude between ground and 6 km altitude for most of the year. Only in
392 April, May and June GEM concentrations decreased with increasing altitude possibly
393 because of the intensive influx of stratospheric air in this season. Gratz et al. (2015)
394 observed in June 2013 high GOM concentrations in tropospheric air mass rich in BrO
395 advected from the subtropical Pacific.
396
397 Opposite to the total GEM depletion reported by Talbot et al. (2007a) our post-flight
398 processed GEM and TM concentrations were never below the detection limit of ~0.05 ng
399 m^{-3}, even at 4 km altitude above the tropopause. However, when using the default Tekran
400 software, small mercury peaks are occasionally not integrated resulting in erroneous zero
401 concentrations. We thus surmise that the zero GEM concentrations reported by Talbot et
402 al. (2007a) were not real but an artifact due to incorrect default integration of the Tekran

raw signal (Swartzendruber et al., 2009; Slemr et al., 2016; Ambrose, 2017). We also note that Talbot et al. (2007a) attribute their measurements to GEM although their inlet system is very similar to that of CARIBIC (Slemr et al., 2014) with proven transmission of GOM. As for CARIBIC, the measurements by Talbot et al. (2007a) are thus more likely close to those of TM.

For the UT Lyman and Jaffe (2012) report Hg^{2+} (GOM + PBM = TM - GEM) concentrations varying between zero and ~ 0.25 ng m^{-3} at TM concentration of ~ 1 ng m^{-3}. High Hg^{2+} concentrations in the UT are inconsistent with our measurements which show comparable GEM and TM concentrations in the UT. Regular vertical profiling of GEM, GOM, and PBM up to 6 km altitude above ground by Brooks et al. (2014) show GOM maxima at ~ 4 km above ground and decreasing GOM concentrations above. Elevated Hg^{2+} concentrations in the UT during the NOMADDS (Nitrogen, Oxidants, Mercury and Aerosol Distributions, Sources and Sinks) campaign were reported by Gratz et al. (2015) but only for an advected tropospheric air mass with high BrO content (Gratz et al., 2015). Based on this information and our own measurements it seems that high GOM concentrations in the UT reported by Lyman and Jaffe (2012) might be an event phenomenon.

As pointed out by Lyman and Jaffe (2012), zero TM concentrations at ~ 2 km above the tropopause from their empirical model do not conform to the observations of significant PBM concentrations in the stratosphere up to 8 km above the tropopause by Murphy et al. (1998, 2006). Gaseous Hg^{2+} (GOM) is assumed to be in equilibrium with PBM. An extrapolation of the equilibria observed at ambient air temperatures near ground (Rutter and Schauer, 2007; Amos et al., 2012) to some -50°C around the tropopause suggests that almost all Hg^{2+} will be attached to particles. Substantial PBM concentrations observed by Murphy et al. (1998, 2006) up to 8 km above the tropopause together with our TM data obtained during some 500 CARIBIC flights (including those with default Tekran raw signal integration) thus exclude the possibility that TM disappears at ~ 2 km above the tropopause. We also note that Murphy et al. (1998, 2006) could not detect any PBM in the troposphere at and below 5 km above ground. Non-detectable PBM in equilibrium with

GOM at still low air temperatures at these altitudes is another piece of evidence inconsistent with generally high GOM concentrations in the UT.

In summary, it is plausible that our TM data currently provide the most representative picture of its UT/LMS distribution and seasonal variation. Our GEM measurements rely on the performance of the GOM quartz wool traps and the difference between TM and GEM is statistically compromised by not being measured along exactly the same routes and altitudes above the tropopause. Despite this, our TM and GEM observations suggest only a small contribution of Hg^{2+} to TM in the UT and are consistent with the observations of substantial PBM concentrations in UT/LS by Murphy et al. (1998, 2006).

3.4 Stratospheric lifetime of TM and GEM

Stratospheric lifetime of a trace gas is defined as atmospheric burden of a compound divided by its stratospheric sink (SPARC Report, Ko et al., eds., 2013). To determine it we use here the relative approach described by Volk et al. (1997) utilizing the CARIBIC N_2O measurements (Assonov et al., 2013) as reference tracer. N_2O, with a lifetime of ~120 yr is nearly uniformly distributed in the troposphere, with little seasonal variation and is only removed in the stratosphere (Nevison et al., 2011). In comparison with SF_6 as chronological tracer, N_2O has the advantage of a much smaller latitudinal gradient in the troposphere and of nearly constant growth rate in the last two decades. Figure 6 shows winter (November – April) average stratospheric TM and GEM concentrations as a function of N_2O mixing ratios. In this plot N_2O mixing ratios were detrended using 2015 as a reference year and the N_2O growth rate of 0.844 ppb yr^{-1} (Assonov et al., 2013).

TM and GEM concentrations in Figure 6 start at 1.18 ± 0.27 (n = 48) and 1.12 ± 0.21 (n = 35) ng m^{-3}, respectively, in the 325 – 330 ppb bin of N_2O mixing ratios and they decrease substantially to 0.59 ± 0.13 (n = 12) and 0.42 ± 0.10 (n = 16) ng m^{-3}, respectively, in the 305 – 310 ppb bin. The difference between TM and GEM concentrations is not statistically significant in the 325 – 330 ppb bin of N_2O mixing ratios, i.e. in the UT as already mentioned before. At lower N_2O mixing ratios, however, GEM concentrations are

systematically smaller than those of TM at the 99% significance level. The TM-GEM difference (i.e. Hg^{2+} concentration in the gas phase (GOM) and on particles (PBM)) is increasing with decreasing N_2O mixing ratios and levels off at ~ 0.17 ng m^{-3} at N_2O mixing ratios below 315 ppb representing ~ 30% of TM concentrations. As mentioned in the experimental section, the CARIBIC trace gas inlet is not optimized for quantitative collection of particles and, consequently, we presume to measure only ~ 70% of Hg^{2+} on particles. If all Hg^{2+} (i.e. TM-GEM) were on particles as predicted by extrapolation of Hg^{2+} gas-particle partitioning equilibrium (Rutter and Schauer, 2007; Amos et al., 2012) from ambient temperature to temperatures at the tropopause then the unbiased Hg^{2+} and TM concentrations would be ~ 0.24 and ~ 0.66 ng m^{-3}, respectively, at N_2O mixing ratios below 310 ppb.

Small decrease of TM and GEM with decreasing N_2O below 315 ppb suggests a long stratospheric lifetime of both TM and GEM. Correlations of all TM and GEM concentrations at N_2O mixing ratios < 315 ppb vs N_2O yield slopes of 6.30 ± 2.96 pg m^{-3} ppb^{-1} (n = 46, R = 0.2947, significance > 95%) and 6.13 ± 1.82 pg m^{-3} ppb^{-1} (n = 63, R = 0.3909, significance > 99%), for TM and GEM, respectively. Using stratospheric N_2O lifetime of 122 ± 24 yr (Volk et al., 1997) we arrive at stratospheric TM and GEM lifetimes of 72 ± 37 and 74 ± 27 yr, respectively. The uncertainties calculated from the slope uncertainties and the uncertainty of N_2O lifetime are probably lower limit because of the narrow range of encountered N_2O mixing ratios in cruising altitudes of the CARIBIC aircraft (Assonov et al., 2013). We note that our stratospheric TM and GEM lifetimes are not “relatively short” as claimed by Lyman and Jaffe (2012). We think that their TM and GEM concentrations were measured within the region of mixing of stratospheric with tropospheric air. Figure 6 shows that TM and GEM vs N_2O correlations would result in much shorter lifetimes when data at N_2O mixing ratios larger than 315 ppb were included. With the calculated uncertainties the stratospheric TM lifetime cannot be distinguished from that of GEM. A more precise estimate of TM and GEM stratospheric lifetimes will require measurements with research aircraft capable of flying at higher altitudes.

Data in Figure 6 allow us to correlate Hg^{2+} (TM - GEM) with GEM as made by Lyman and Jaffe (2012). Hg^{2+} is negatively correlated with GEM with a slope of -0.13 ± 0.04 (n = 7, R^2 = 0.712) and -0.31 ± 0.04 (n = 7, R^2 = 0.919) when averages and medians are used, respectively. Chemical conversion of GEM into Hg^{2+} without any Hg^{2+} losses would yield a slope of -1 and slopes near this value were reported for the free troposphere by Swartzendruber et al. (2006) and for the UT by Lyman and Jaffe (2012). Our negative slopes in the stratosphere are substantially greater than -1 and somewhat greater than -0.53 reported by Lyman and Jaffe (2012) for stratosphere-influenced air masses. Negative slopes greater than -1 imply losses of Hg^{2+} (Hg^{2+} yield of GEM oxidation is smaller than the stoichiometry of the reaction) and result in decreasing TM concentrations with increasing Hg^{2+} concentrations in the stratosphere.

A reduction of TM concentration from ~ 1.2 ng m^{-3} in tropospheric air to ~ 0.66 ng m^{-3} in stratospheric air is too large to be explained by the aerosol bias induced by the incomplete particle sampling mentioned above and requires Hg^{2+} removal process. As already proposed by Lyman and Jaffe (2012) such removal process requires an oxidation of GEM into Hg^{2+}, an attachment of Hg^{2+} to abundant stratospheric, mainly sulfate, particles, and their removal by gravitational sedimentation and/or scavenging by clouds (Menzies and Tratt, 1995; Rasch et al., 2008; Wilson et al., 2008). We note that air mass exchange is also taking important part in removing the sulfate particles from the stratosphere but TM concentrations would not change without sedimentation and scavenging of Hg^{2+} on particles. The oxidation and subsequent attachment to particles could be a local process in the vicinity of extratropical tropopause layer (exTL) or a non-local process in the tropical upper troposphere (TTL) and during the transport from the TTL to the location of the IAGOS-CARIBIC measurements in the LMS.

If all stratospheric TM were Hg^{2+} and attached to particles then the stratospheric lifetime of TM would be given by the stratospheric lifetime of particles of several years (Waugh and Hall, 2002; Friberg et al., 2018). Substantially longer TM and GEM stratospheric lifetimes of ~70 yr suggest that the stratospheric GEM is oxidized higher up in the stratosphere (Ko et al., 2013). Our TM and GEM stratospheric lifetimes are comparable to

COS lifetime of 64 ± 21 yr (Barkley et al., 2008) whose oxidation by photolysis and the reaction with $O(^3P)$ in the stratosphere is located predominantly in tropics at an altitude of ~30 km (Brühl et al., 2012). Long stratospheric lifetimes are governed by the rate of delivery of a substance to its loss region (Ko et al., 2013). Comparable stratospheric lifetimes of TM, GEM, and COS thus suggest a similar location of their stratospheric loss regions. At ~30 km altitude GEM could be oxidized by Br atoms released by the photolysis of halons and/or by reactions with O atoms (Ko et al., 2013). Collocation of stratospheric loss regions of COS and GEM supports the hypothesis of close relation of stratospheric mercury to stratospheric sulfur (COS + sulfate particles) as described by Wilson et al. (2008).

Conclusions and outlook

The obvious implication of the long stratospheric TM and GEM lifetimes is that most atmospheric mercury is oxidized in the troposphere. The second direct implication is that if the lifetime of GEM in the stratosphere with its very high O_3 mixing ratios (typically 1 ppm and more) is quite long, then the GEM + O_3 reaction cannot be important in the troposphere with its low O_3 mixing ratios. This implies that either the reaction does not take place or that the primary reaction product is instable. Moreover, with very low stratospheric H_2O mixing ratios below 10 ppm, OH is also an unlikely oxidant for GEM in the stratosphere. The most plausible remaining stratospheric oxidants are Br atoms originating from the decomposition of halons with a possible contribution of O atoms.

The regular intercontinental IAGOS-CARIBIC flights provide an insight into the large-scale distribution of TM and GEM in the UT/LMS and its seasonal variation. Post-flights processed data with better accuracy and higher precision reveal a seasonal variation of vertical TM distribution in the UT/LMS which is similar to most of the trace gases with sources in the troposphere, such as CH_4 and CO. Importantly, even at altitudes of up to 3.5 km above the thermal tropopause TM concentrations are still ~0.5 ng m^{-3}, one order of magnitude above the instrumental detection limit. We have never observed zero TM or

GEM concentrations and attribute earlier reports about them to an insufficiency in the default signal integration of the Tekran instrument.

Latitudinal TM distribution in the UT during the flights to South America and South Africa were found to be strongly influenced by biomass burning. Although TM and GEM were not measured at the same place and at the same time, the data collectively show that their concentrations in the UT are similar and the Hg^{2+} concentrations are thus usually small. Recent reports on high GOM and Hg^{2+} concentrations in the free troposphere are limited to middle tropospheric altitudes (Brooks et al., 2014), to an event with high BrO concentrations (Gratz et al., 2015) or to a stratospheric intrusion (Lyman and Jaffe, 2012) and are in view of our observational IAGOS-CARIBIC data set most likely not representative for large-scale UT distribution. Larger Hg^{2+} (TM – GEM) concentrations of up to about half of TM concentrations were observed only in the LMS.

Lower TM concentrations were generally observed in LMS with the pronounced gradient just above the tropopause. We attribute this gradient to mixing of tropospheric air with stratospheric air depleted of mercury. The conservative character of TM measurements implicates thus a loss process by oxidation to Hg^{2+}, its attachment to particles and their subsequent removal by gravitational sedimentation and/or scavenging by clouds. Substantial stratospheric PBM concentrations reported by Murphy et al. (1998, 2006) and GOM/PBM equilibria (Rutter and Schauer, 2007; Amos et al., 2012) extrapolated to temperatures in the LMS support this hypothesis.

Correlations of TM and GEM with N_2O as a reference substance show statistically the same TM and GEM concentrations in the UT. In the N_2O range of 330 and 315 ppb TM and GEM concentrations rapidly decrease with decreasing N_2O mixing ratios due to mixing of tropospheric air with stratospheric air depleted of mercury. Below 315 ppb until 295 ppb of N_2O, TM and GEM concentrations hardly change. TM and GEM lifetimes of 72 ± 37 and 74 ± 27 yr, respectively, were calculated from correlations of TM and GEM vs N_2O below 315 ppb, albeit with large uncertainties caused by the limited altitude range of commercial airliners and the resulting narrow range of N_2O mixing ratios between 315 and

295 ppb. Measurements of TM, GEM, and N_2O to higher altitudes above the tropopause (i.e. to N_2O mixing ratios substantially below 290 ppb) are needed to better constrain the stratospheric TM and GEM lifetimes.

Stratospheric lifetimes of TM and GEM are comparable to the COS stratospheric lifetime of 64 ± 21 yr (Barkley et al., 2008), which is in volcanically quiet periods the major precursor of sulfate particles in the stratosphere (Wilson et al., 2008). Comparable COS and GEM stratospheric lifetimes suggest collocation of their loss regions. This coincidence corroborates the hypothesis of Hg^{2+} attachment to sulfate particles and their removal by gravitational sedimentation and scavenging by clouds. This hypothesis, first proposed by Lyman and Jaffe (2012), could be directly tested in future by quantitative measurements of Hg/S ratios on stratospheric particles. Such measurements would also better constrain the mercury fluxes across the tropopause.

Mercury measurements onboard IAGOS-CARIBIC were stopped in March 2016 and the space of the mercury instrument is now occupied by other instruments. The reason for the termination of the mercury measurements was the feeling that, with the present instrumentation, we will only reproduce the existing data. An improved instrumentation including reliable speciation technique is needed to gain new insights. Any institution capable of providing and maintaining such an instrument is welcomed to participate in future IAGOS-CARIBIC measurements. For details please consult the CARIBIC coordinator Andreas Zahn.

Acknowledgements

We thank Lufthansa Airlines and Lufthansa Technik for their commitment and support. We also thank Jan Boedewadt from HZG for modifying the Tekran instrument for deployment in the CARIBIC container. The development and operation of the CARIBIC system has been financially supported by the German Ministry of Education and Science (AFO 2000, IAGOS-D), by the European Commission's DGXII Environment RTD 4th

and 5th Framework programs, by grants from the Max Planck Society and from Frankfurt Airport.

References

AMAP/UNEP: Technical Background Report for the Global Mercury Assessment, 2013, available at AMAP (www.amap.no) and UNEP Chemicals Branch´s (http://www.unep.org/hazardoussubstances/mercury/informationmaterials/reportsandpublications/tabid/3593/default.aspx) websites.

Ambrose, J.L., Gratz, L.E., Jaffe, D.A., Campos, T., Flocke, F.M., Knapp, D.J., Stechman, D.M., Stell, M., Weinheimer, A.J., Cantrell, C.A., and Mauldin III, R.L.: Mercury emission ratios from coal-fired power plants in the southeastern United States during NOMADDS, Environ. Sci. Technol., 49, 10389-10397, 2015.

Ambrose, J.L.: Improved methods for signal processing in measurements of mercury by Tekran 2537A and 2537B instruments, Atmos. Meas. Tech., 10, 5063-5073, 2017.

Amos, H.M., Jacob, D.J., Holmes, C.D., Fisher, J.A., Wang, Q., Yantosca, R.M, Corbitt, E.S., Galarneau, E., Rutter, A.P., Gustin, M.S., Steffen, A., Schauer, J.J., Graydon, J.A., Louis, V.L.St., Talbot, R.W., Edgerton, E.S., Zhang, Y., and Sunderland, E.M.: Gas-particle partitioning of atmospheric Hg(II) and its effect on global mercury deposition, Atmos. Chem. Phys., 12, 591-603, 2012.

Andreae, M.O., and Merlet, P.: Emission of trace gases and aerosols from biomass burning, Global Biogeochem. Cycles, 15, 955-966, 2001.

Ariya, P.A., Amyot, M., Dastoor, A., Deeds, D., Feinberg, A., Kos, G., Poulain, A., Ryjkov, A., Semeniuk, K., Subir, M., and Toyota, K.: Mercury physicochemical and biogeochemical transformation in the atmosphere and at atmospheric interfaces: A review and future direction, Chem. Rev., 115, 3760-3802, 2015.

649 Assonov, S.S., Brenninkmeijer, C.A.M., Schuck, T., and Umezawa, T.: N_2O as a tracer of
650 mixing stratospheric and tropospheric air based on CARIBIC data with applications for
651 CO_2, Atmos. Environ., 79, 769-779, 2013.
652
653 Banic, C.M., Beauchamp, S.T., Tordon, R.J., Schroeder, W.H., Steffen, A., Anlauf, K.A.,
654 and Wong, K.H.T.: Vertical distribution of gaseous elemental mercury in Canada, J.
655 Geophys. Res., 108 (D9), 4264, doi:10.1029/2002JD002116, 2003.
656
657 Barkley, M.P., Palmer, P.I., Boone, C.D., Bernath, P.F., and Sunthralanigam, P.: Global
658 distributions of carbonyl sulfide in the upper troposphere and stratosphere, Geophys. Res.
659 Lett., 35, L14810, doi:10.1029/2008GL034270, 2008.
660
661 Baron, P. A., and Willeke K.: Aerosol Measurements: Principles, Techniques and
662 Applications, John Wiley and Sons, New York, 1131 pp, 2001.
663
664 Bieser, J., Slemr, F., Ambrose, J., Brenninkmeijer, C., Brooks, S., Dastoor, A., DeSimone,
665 F., Ebinghaus, R., Gencarelli, C.N., Geyer, B., Gratz, L.E., Hedgecock, I.M., Jaffe, D.,
666 Kelley, P., Lin, C.-J., Jaegle, L., Matthias, V., Ryjkov, A., Selin, N.E., Song, S., Travnikov,
667 O., Weigelt, A., Luke, W., Ren, X., Zahn, A., Yang, X., Zhu, Y., and Pirrone, N.: Multi-
668 model study of mercury dispersion in the atmosphere: vertical and interhemispheric
669 distribution of mercury species, Atmos. Chem. Phys., 17, 6925-6955, 2017.
670
671 Brenninkmeijer, C.A.M., Crutzen, P., Boumard, F., Dauer, T., Dix, B., Ebinghaus, R.,
672 Filippi, D., Fischer, H., Franke, H., Frieß, U., Heintzenberg, J., Helleis, F., Hermann, M.,
673 Kock, H.H., Koeppel, C., Lelieveld, J., Leuenberger, M., Martinsson, B.G., Miemczyk, S.,
674 Moret, H.P., Nguyen, H.N., Nyfeler, P., Oram, D., O'Sullivan, D., Penkett, S., Platt, U.,
675 Pupek, M., Ramonet, M., Randa, B., Reichelt, M., Rhee, T.S., Rohwer, J., Rosenfeld, K.,
676 Scharffe, D., Schlager, H., Schumann, U., Slemr, F., Sprung, D., Stock, P., Thaler, R.,
677 Valentino, F., van Velthoven, P., Waibel, A., Wandel, A., Waschitschek, K., Wiedensohler,
678 A., Xueref-Remy, I., Zahn, A., Zech, U., and Ziereis, H.: Civil aircraft for the regular

679 investigation of the atmosphere based on an instrumented container: The new CARIBIC
680 system, Atmos. Chem. Phys., 7, 1-24, 2007.
681
682 Brooks, S., Ren, X., Cohen, M., Luke, W.T., Kelley, P., Artz, R., Hynes, A., Landing, W.,
683 and Martos, B.: Airborne vertical profiling of mercury speciation near Tullahoma, TN,
684 USA, Atmosphere, 5, 557-574, 2014.
685
686 Brühl, C., Lelieveld, J., Crutzen, P.J., and Tost, H.: The role of carbonyl sulfide as a source
687 of stratospheric sulfate aerosol and its impact on climate, Atmos. Chem. Phys., 12, 1239-
688 1253, 2012.
689
690 Brunke, E.-G., Labuschagne, C., and Slemr, F.: Gaseous mercury emissions from a fire in
691 the Cape Peninsula, South Africa, during January 2000, Geophys. Res. Lett., 28, 1483-
692 1486, 2001.
693
694 Dibble, T.S., Zelie, M.J., and Mao, H.: Thermodynamics of reactions of ClHg and BrHg
695 radicals with atmospherically abundant free radicals, Atmos. Chem. Phys., 12, 10271-
696 10279, 2012.
697
698 Duncan, B.R., Martin, R.V., Staudt, A.C., Yevich, R., and Logan, J.A.: Interannual and
699 seasonal variability of biomass burning emissions constrained by satellite observations, J.
700 Geophys. Res., 108, doi: 10.1029/2002JD002378, 2003.
701
702 Ebinghaus, R. and Slemr, F.: Aircraft measurements of atmospheric mercury over southern
703 and eastern Germany, Atmos. Environ., 34, 895-903, 2000.
704
705 Ebinghaus, R., Slemr, F., Brenninkmeijer, C.A.M., van Velthoven, P., Zahn, A., Hermann,
706 M., O´Sullivan, D.A., and Oram, D.E.: Emissions of gaseous mercury from biomass
707 burning in South America in 2005 observed during CARIBIC flights, Geophys. Res. Lett.,
708 34, L08813, doi:10.1029/2006GL028866, 2007.
709

710 Friberg, J., Martinsson, B.G., Andersson, S.M., and Sandvik, O.S.: Volcanic impact on the
711 climate – the stratospheric aerosol load in the period 2006 – 2015, Atmos. Chem. Phys.
712 Discuss., doi:10.5194/acp-2017-1200.
713
714 Friedli, H.R., Radke, L.F., and Yu, J.Y.: Mercury in smoke from biomass fires, Geophys.
715 Res. Lett., 28, 3223-3226, 2001.
716
717 Friedli, H.R., Radke, L.F., Lu, J.Y., Banic, C.M., Leaitch, W.R., and MacPherson, J.I.:
718 Mercury emissions from burning of biomass from temperate North American forests:
719 laboratory and airborne measurements, Atmos. Environ., 37, 253-267, 2003a.
720
721 Friedli, H.R., Radke, L.F., Prescott, R., Hobbs, P.V., and Sinha, P.: Mercury emissions
722 from the August 2001 wildfires in Washington State and an agricultural waste fire in
723 Oregon and atmospheric mercury budget estimates, Global Biogeochem. Cycles, 17,
724 doi:10.1029/2002GB001972, 2003b.
725
726 Friedli, H.R., Radke, L.F., Prescott, R., Li, P., Wo, J.-H., and Carmichael, G.R.: Mercury
727 in the atmosphere around Japan, Korea, and China as observed during the 2001 ACE-Asia
728 field campaign: Measurements, distributions, sources, and implications, J. Geophys. Res.,
729 109, D19S25, doi:10.1029/2003JD004244, 2004.
730
731 Friedli, H.R., Arellano, A.F., Cinnirella, S., and Pirrone, N.: Initial estimates of mercury
732 emissions to the atmosphere from global biomass burning, Environ. Sci. Technol., 43,
733 3507-3513, 2009.
734
735 Gettelman, A., Hoor, P., Pan, L.L., Randel, W.J., Hegglin, M.I., and Birner, T.: The
736 extratropical upper troposphere and lower stratosphere, Rev. Geophys., 49, RG3003,
737 doi:10.1029/2011RG000355, 2011.
738
739 Gratz, L.E., Ambrose, J.L., Jaffe, D.A., Shah, V. Jaeglé, L., Stutz, J., Festa, J., Spolaor, M.,
740 Tsai, C., Selin, N.E., Song, S., Zhou, X., Weinheimer, A.J., Knapp, D.J., Montzka, D.D.,

741 Flocke, F.M., Campos, T.L., Apel, E., Hornbrook, R., Blake, N.J., Hall, S., Tyndall, G.S.,
742 Reeves, M., Stechman, D., and Stell, M.: Oxidation of mercury by bromine in the
743 subtropical Pacific free troposphere, Geophys. Res. Lett., 42, doi:10.1002/2015GL066645,
744 2015.
745
746 Gustin, M.S., Amos, H.M., Huang, J., Miller, M.B., and Heidecorn, K.: Measuring and
747 modeling mercury in the atmosphere: a critical review, Atmos. Chem. Phys., 15, 5697-
748 5713, 2015.
749
750 Holmes, C.D., Jacob, D.J., Corbitt, E.S., Mao, J., Yang, X., Talbot, R., and Slemr, F.:
751 Global atmospheric model for mercury including oxidation by bromine atoms, Atmos.
752 Chem. Phys., 10, 12037-12057, 2010.
753
754 Holton, J.R., Haynes, P.H., McIntyre, M.E., Douglass, A.R., Rood, R.B., and Pfister, L.:
755 Stratosphere-troposphere exchange, Rev. Geophys., 33, 403-439, 1995.
756
757 Horowitz, H.M., Jacob, D.J., Zhang, Y., Dibble, T.S., Slemr, F., Amos, H.M., Schmidt,
758 J.A., Corbitt, E.S., Marais, E.A., and Sunderland, E.M.: A new mechanism for atmospheric
759 mercury redox chemistry: Implications for the global mercury budget, Atmos. Chem.
760 Phys., 17, 6353-6371, 2017.
761
762 Kaiser, R., and Gottschalk, G.: Elementare Tests zur Beurteilung von Meßdaten,
763 Bibliographisches Institut, Mannheim, 1972.
764
765 Ko, M.K.W., Newman, P.A., Reimann, S., and Strahan, S.E., eds.: Lifetimes of
766 stratospheric ozone-depleting substances, their replacements, and related species, SPARC
767 Report No. 6, WCRP-15/2013, December 2013.
768
769 Kunz, A., Konopka, P., Müller, R., and Pan, L.L.: Dynamical tropopause based on
770 isentropic potential vorticity gradients, J. Geophys. Res., 116, D01110,
771 doi:10.1029/2010JD014343, 2011.

Lin, C.-J., Pongprueksa, P., Lindberg, S.E., Pehkonen, S.O., Byun, D., and Jang, C.: Scientific uncertainties in atmospheric mercury models. I. Model science evaluation, Atmos. Environ, 40, 2911-2928, 2006.

Lindberg, S., Bullock, R., Ebinghaus, R., Engstrom, D., Feng, X., Fitzgerald, W., Pirrone, N., Prestbo, E., and Seigneur, C.: A synthesis of progress and uncertainties in attribution the sources of mercury in deposition, Ambio, 36, 19-32, 2007.

Lyman, S.N., and Jaffe, D.A.: Formation and fate of oxidized mercury in the upper troposphere and lower stratosphere, Nature Geosci., 5, 114-117, 2012.

Menzies, R.T., and Tratt, D.M.: Evidence of seasonally dependent stratosphere-troposphere exchange and purging of lower stratospheric aerosol from a multiyear lidar data set, J. Geophys. Res., 100, D2, 3139-3148, 1995.

Mergler, D., Anderson, H.A., Chan, L.H.M., Mahaffey, K.R., Murray, M., Sakamoto, M., and Stern, A.H.: Methyl mercury exposure and health effects in humans: A worldwide concern, Ambio, 36, 3-11, 2007.

Murphy, D.M., Thomson, D.S., and Mahoney, M.J.: In situ measurements of organics, meteoritic material, mercury, and other elements in aerosols at 5 to 19 kilometers, Science, 282, 1664-1669, 1998.

Murphy, D.M., Hudson, P.K., Thomson, D.S., Sheridan, P.J., and Wilson, J.C.: Observations of mercury-containing aerosols, Environ. Sci. Technol., 40, 3163-3167, 2006.

Nevison, C.D., Dlugokencky, E., Dutton, G., Elkins, J.W., Fraser, P., Hall, B., Krummel, P.B., Langenfelds, R.L., O´Doherty, S., Prinn, R.G., Steele, L.P., and Weiss, R.F.:

802 Exploring causes of interannual variability in the seasonal cycles of tropospheric nitrous
803 oxide, Atmos. Chem. Phys., 11, 3713-3730, 2011.
804
805 Pirrone, N., Cinnirella, S., Feng, X., Finkelman, R.B., Friedli, H.R., Leaner, J., Mason, R.,
806 Mukherjee, A.B., Stracher, G.B., Streets, D.G., and Telmer, K.: Global mercury emissions
807 to the atmosphere from anthropogenic and natural sources, Atmos. Chem. Phys., 10, 5951-
808 5964, 2010.
809
810 Radke, L.F., Friedli, H.R., and Heikes, B.G.: Atmospheric mercury over the NE Pacific
811 during spring 2002: Gradients, residence time, upper troposphere lower stratosphere loss,
812 and long-range transport, J. Geophys. Res., 112, D19305, doi:10.1029/2005JD005828,
813 2007.
814
815 Rasch, P.J., Tilmes, S., Turco, R.P., Robock, A., Oman, L., Chen, C.-C., Stenchikov, G.L.,
816 and Garcia, R.R.: An overview of geoengineering of climate using stratospheric sulphate
817 aerosols, Phil. Trans. R. Soc. A, 366, 4007-4037, 2008.
818
819 Rutter, A.P., and Schauer, J.J.: The effect of temperature on the gas-particle partitioning of
820 reactive mercury in atmospheric aerosols, Atmos. Environ., 41, 8647-8657, 2007.
821
822 Scheele, M., Siegmund, P., and Van Velthoven, P.: Sensitivity of trajectories to data
823 resolution and its dependence on the starting point: In or outside a tropopause fold,
824 Meteorol. Appl., 3, 267-273, 1996.
825
826 Scheuhammer, A.M., Meyer, M.W., Sandheinrich, M.B., and Murray, M.W.: Effects of
827 environmental methylmercury on the health of wild bird, mammals, and fish, Ambio, 36,
828 12-18, 2007.
829
830 Selin, N.E., Jacob, D.J., Park, R.J., Yantosca, R.M., Strode, S., Jaeglé, L., and Jaffe, D.:
831 Chemical cycling and deposition of atmospheric mercury: Global constraints from
832 observations, J. Geophys. Res., 112, D02308, doi:10.1029/2006JD007450, 2007.

Slemr, F., Ebinghaus, R., Brenninkmeijer, C.A.M., Hermann, M., Kock, H.H., Martinsson, B.G., Schuck, T., Sprung, D., van Velthoven, P., Zahn, A., and Ziereis, H.: Gaseous mercury distribution in the upper troposphere and lower stratosphere observed onboard the CARIBIC passenger aircraft, Atmos. Chem. Phys., 9, 1957-1969, 2009.

Slemr, F., Weigelt, A., Ebinghaus, R., Brenninkmeijer, C., Baker, A., Schuck, T., Rauthe-Schöch, A., Riede, H., Leedham, E., Hermann, M., van Velthoven, P., Oram, D., O´Sullivan, D., Dyroff, C., Zahn, A., and Ziereis, H.: Mercury plumes in the global upper troposphere observed during flights with the CARIBIC observatory from May 2005 until June 2013, Atmosphere 5, 342-369, 2014.

Slemr, F., Weigelt, A., Ebinghaus, R., Kock, H.H., Bödewadt, J., Brenninkmeijer, C.A.M., Rauthe-Schöch, A., Weber, S., Hermann, M., Becker, J., Zahn, A., and Martinsson, B.: Atmospheric mercury measurements onboard the CARIBIC passenger aircraft, Atmos. Meas. Tech., 9, 2291-2302, 2016.

Sprovieri, F., Pirrone, N., Ebinghaus, R., Kock, H., and Dommergue, A: A review of worldwide atmospheric mercury measurements, Atmos. Chem. Phys., 10, 8245-8265, 2010.

Sprung, D., and Zahn, A.: Acetone in the upper troposphere/lowermost stratosphere measured by the CARIBIC passenger aircraft: Distribution, seasonal cycle, and variability, J. Geophys. Res., 115, D16301, doi:10.1029/2009JD012099, 2010.

Swartzendruber, P.C., Jaffe, D.A., Prestbo, E.M., Weiss-Penzias, P., Selin, N.E., Park, R., Jacob, D.J., Strode, S., and Jaeglé, L.: Observations of reactive gaseous mercury in the free troposphere at the Mount Bachelor Observatory, J. Geophys. Res., 111, D24301, doi:10.1029/2006JD007415, 2006.

Swartzendruber, P.C., Chand, D., Jaffe, D.A., Smith, J., Reidmiller, D., Gratz, L., Keeler, J., Strode, S., Jaeglé, L., and Talbot, R.: Vertical distribution of mercury, CO, ozone, and aerosol scattering coefficient in the Pacific Northwest during the spring 2006 INTEX-B campaign, J. Geophys. Res., 113, D10305, doi:10.1029/2007JD009579, 2008.

Swartzendruber, P.C., Jaffe, D.A., and Finley, B.: Improved fluorescence peak integration in the Tekran 2537 for applications with sub-optimal sample loadings, Atmos. Environ., 43, 3648-3651, 2009.

Talbot, R., Mao, H., Scheuer, E., Dibb, J., and Avery, M.: Total depletion of Hg^0 in the upper troposphere – lower stratosphere, Geophys. Res. Lett., 34, L23804, doi:10.1029/2007GL031366, 2007a.

Talbot, R., Mao, H., Scheuer, E., Dibb, J., Avery, M., Browell, E., Sachse, G., Vay, S., Blake, D., Huey, G., and Fuelberg, H.: Factors influencing the large-scale distribution of Hg^o in the Mexico City area and over the North Pacific, Atmos. Chem. Phys. Discuss., 7, 15533-15563, 2007b.

Travnikov, O., Angot, H., Artaxo, P., Bencardino, M., Bieser, J., D´Amore, F., Dastoor, A., De Simone, F., Carmen Diéguez, M., Dommergue, A., Ebinghaus, R., Feng, X.B., Gencarelli, C.N., Hedgecock, I.M., Magand, O., Martin, L., Matthias, V., Mashyanov, N., Pirrone, N., Ramachandran, R., Read, K.A., Ryjkov, A., Selin, N.E., Sena, F., Song, S., Sprovieri, F., Wip, D., Wängberg, I., and Yang, X.: Multi-model study of mercury dispersion in the atmosphere: atmospheric processes and model evaluation, Atmos. Chem. Phys., 17, 5271-5295, 2017.

Volk, C.M., Elkins, J.W., Fahey, D.W., Dutton, G.S., Gilligan, J.M., Loewenstein, M., Podolske, J.R., Chan, K.R., and Gunson, M.R.: Evaluation of source gas lifetimes from stratospheric observations, J. Geophys. Res. 102, D21, 25543-25564, 1997.

Waugh, D.W., and Hall, T.M.: Age of stratospheric air: Theory, observations, and models, Rev. Geophys. 40, doi:10.1029/2000RG000101, 2002.

Weigelt, A., Ebinghaus, R., Pirrone, N., Bieser, J., Bödewadt, J., Esposito, G., Slemr, F., van Velthoven, P.F.J., Zahn, A., and Ziereis, H.: Tropospheric mercury vertical profiles between 500 and 10000 m in central Europe, Atmos. Chem. Phys., 16, 4135-4146, 2016a.

Weigelt, A., Slemr, F., Ebinghaus, R., Pirrone, N., Bieser, J., Bödewadt, J., Esposito, G., and van Velthoven, P.F.J.: Mercury emissions of a coal-fired power plant in Germany, Atmos. Chem. Phys., 16, 13653-13668, 2016b.

Wilson, J.C., Lee, S.-H., Reeves, J.M., Brock, C.A., Jonsson, H.H., Lafleur, B.G., Loewenstein, M., Podolske, J., Atlas, E., Boehring, K., Toon, G., Fahey, D., Bui, T.P., Diskin, G., and Moore, F.: Steady-state aerosol distributions in the extra-tropical, lower stratosphere and the processes that maintain them, Atmos. Chem. Phys., 8, 6617-6626, 2008.

Figures

Figure 1: Tracks of the CARIBIC flights made beetween April 2014 and February 2016 (CARIBIC flights #468-536). Mercury data for these flights were obtained by post-flight processing of the Tekran raw signal (Slemr et al., 2016).

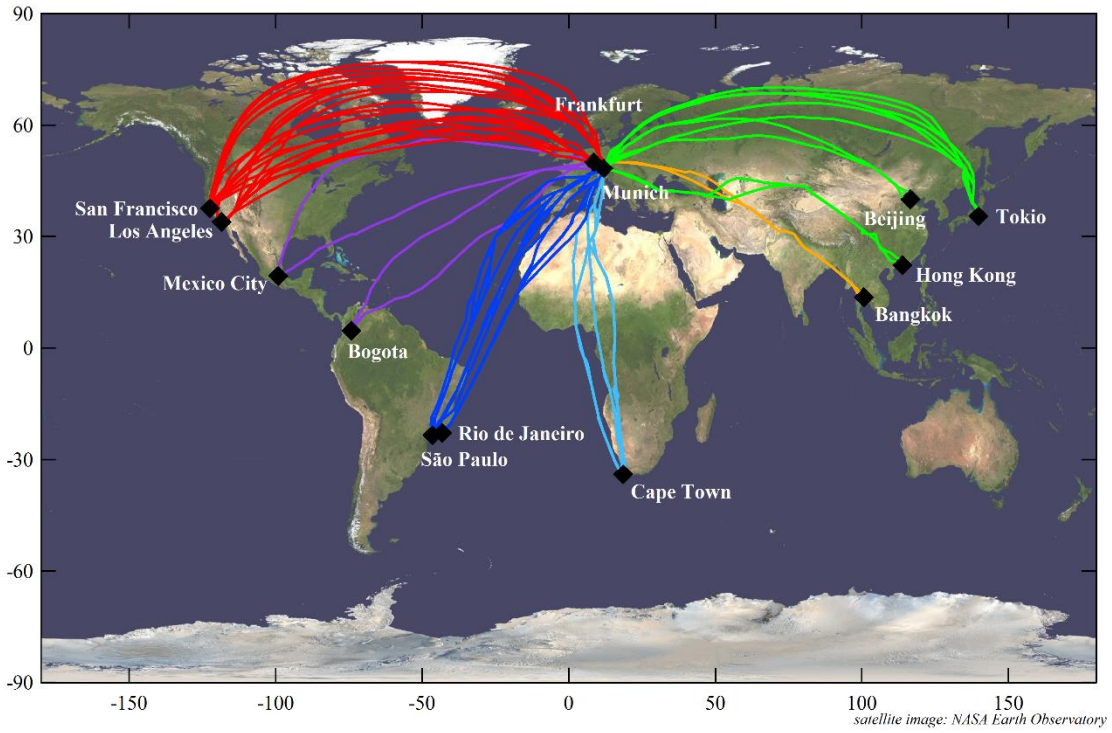

Figure 2: Latitudinal distributions of tropospheric (PV ≤ 1.5 PVU) TM, CO, CH_4, and acetonitrile (AN) during the flights from Bogota and São Paulo/Rio de Janeiro to Munich in summer (only July and August, JA), autumn (September, October, and November, SON) and winter (December, January, and February, DJF). The points represent averages and the vertical bars their standard error. No acetonitrile data were available south of 20°S.

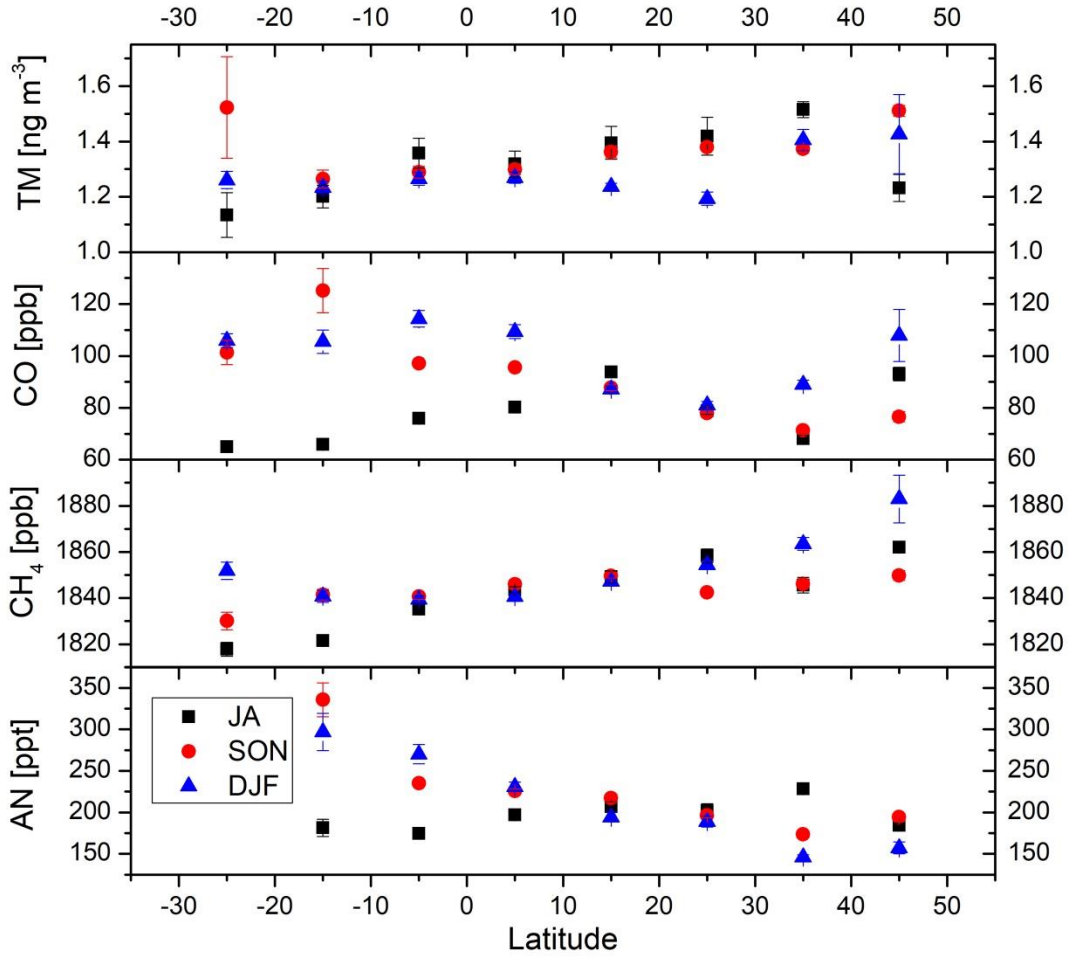

929 Figure 3: Latitudinal distributions of tropospheric TM, CO, CH_4, and acetonitrile (AN) in
930 winter (December, January, and February, DJF) during the flights from Cape Town and
931 São Paulo to Munich. The points represent averages and the vertical bars their standard
932 error. No acetonitrile data are available south of 30°S and 20°S for flights to Cape Town
933 and São Paulo, respectively.
934

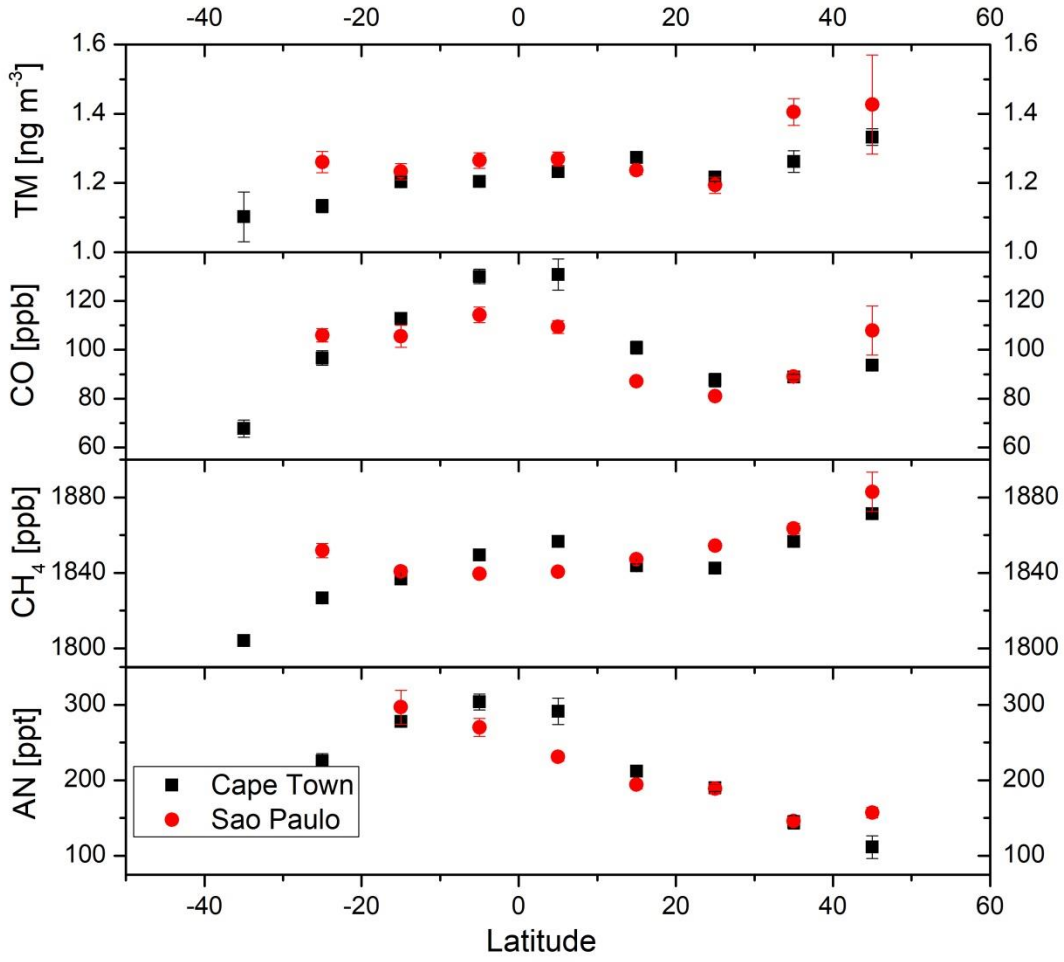

935
936

Figure 4: Seasonal variation of mean TM concentrations (a), CO (b), CH_4 (c) and O_3 (d) mixing ratios in distance relative to the thermal tropopause derived from ozone soundings according to Sprung and Zahn (2010). All TM data north of 20°N obtained between April 2014 and February 2016 were considered for this plot (2288 individual data points).

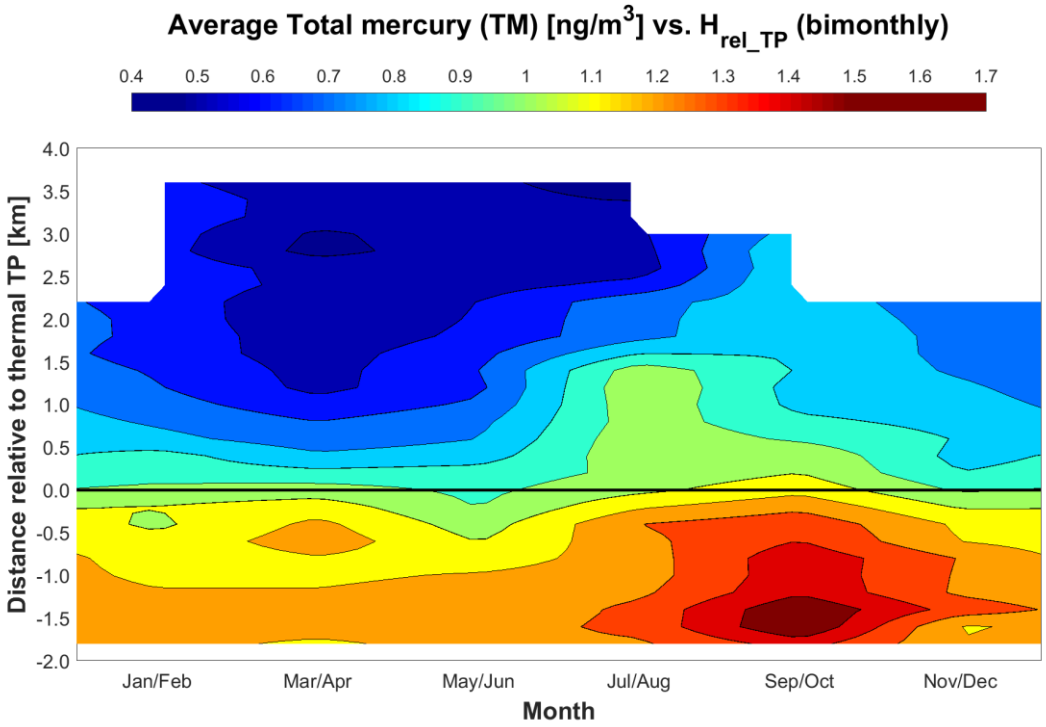

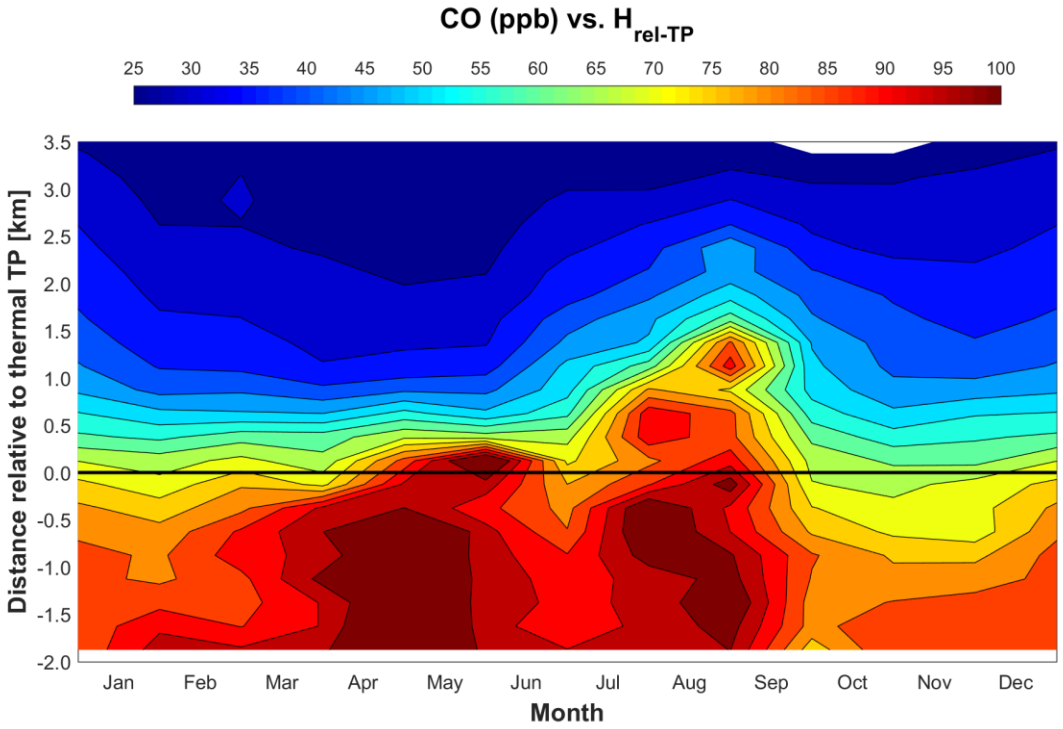

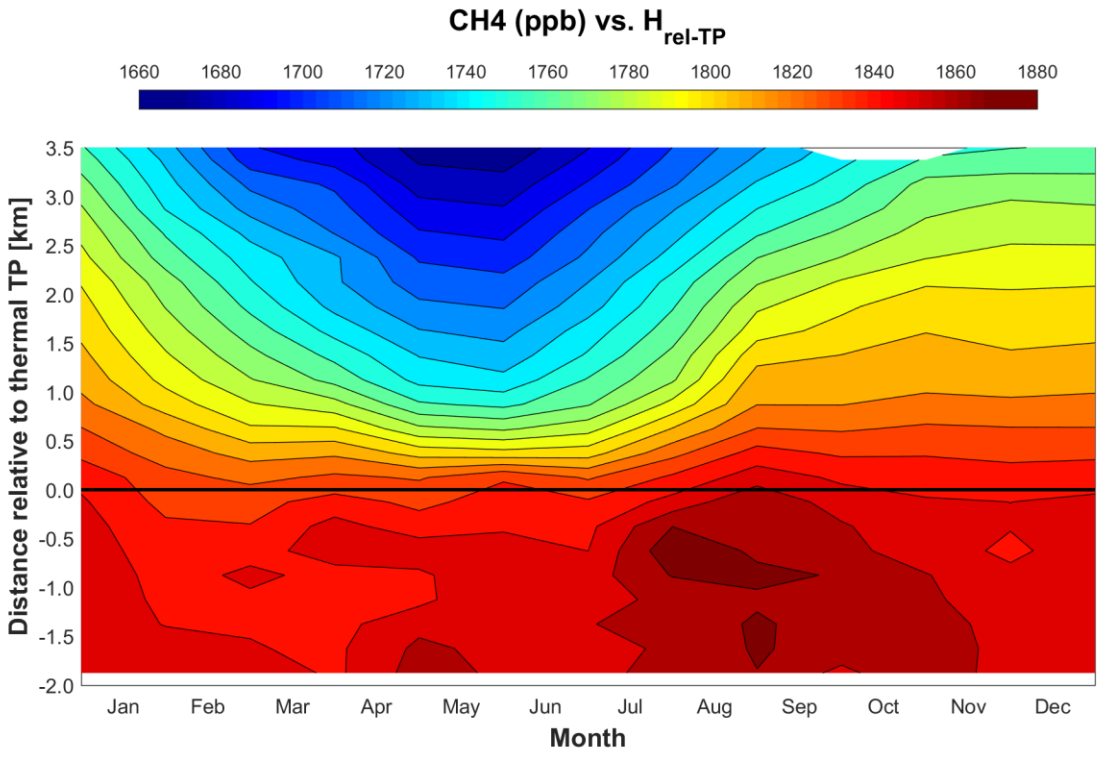
CH4 (ppb) vs. H rel-TP
1660 1680 1700 1720 1740 1760 1780 1800 1820 1840 1860 1880
Distance relative to thermal TP [km]
3.5 3.0 2.5 2.0 1.5 1.0 0.5 0.0 -0.5 -1.0 -1.5 -2.0
Jan Feb Mar Apr May Jun Jul Aug Sep Oct Nov Dec
Month

945
946

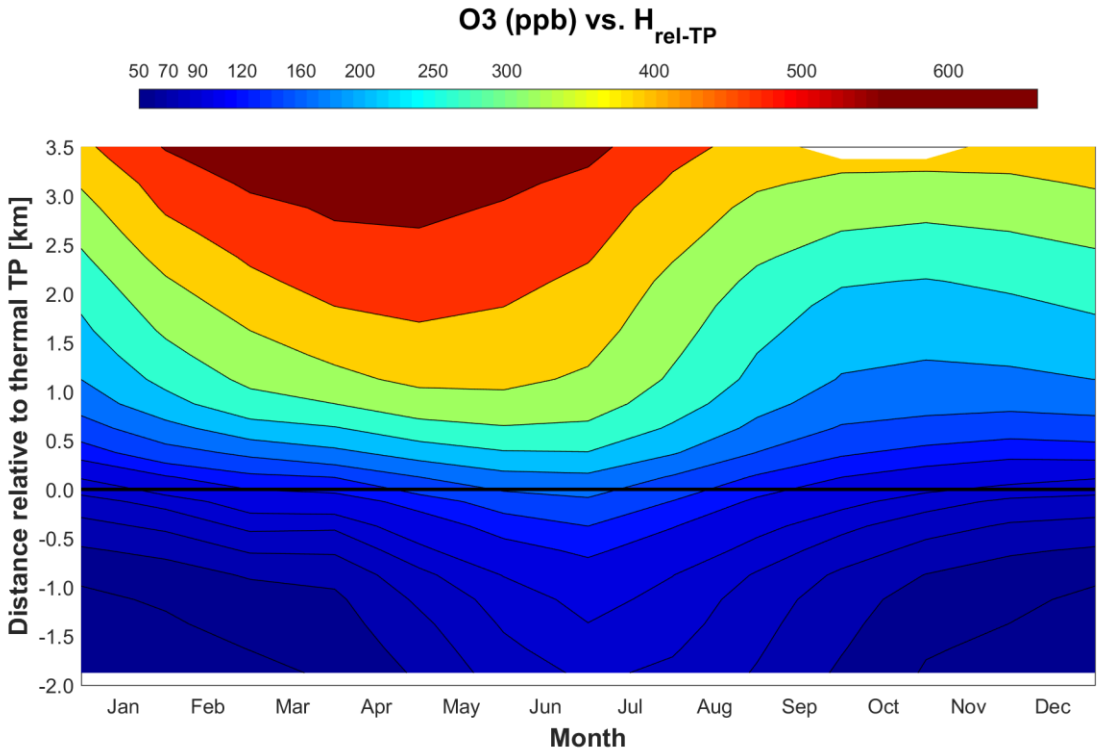
O3 (ppb) vs. H rel-TP
50 70 90 120 160 200 250 300 400 500 600
Distance relative to thermal TP [km]
3.5 3.0 2.5 2.0 1.5 1.0 0.5 0.0 -0.5 -1.0 -1.5 -2.0
Jan Feb Mar Apr May Jun Jul Aug Sep Oct Nov Dec
Month

947

Figure 5: Vertical TM and GEM distribution relative to the thermal tropopause in a) winter (December – May, upper panel) and b) in summer (June – November, lower panel). The data points represent averages and their standard errors, extreme values were eliminated using the Nalimov outlier test (Kaiser and Gottschalk, 1972).

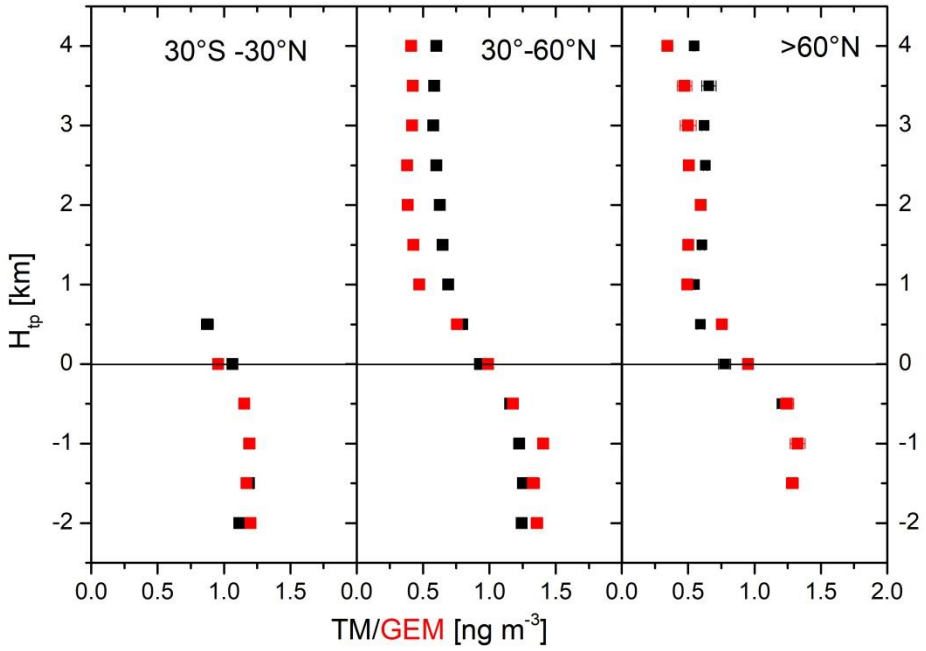

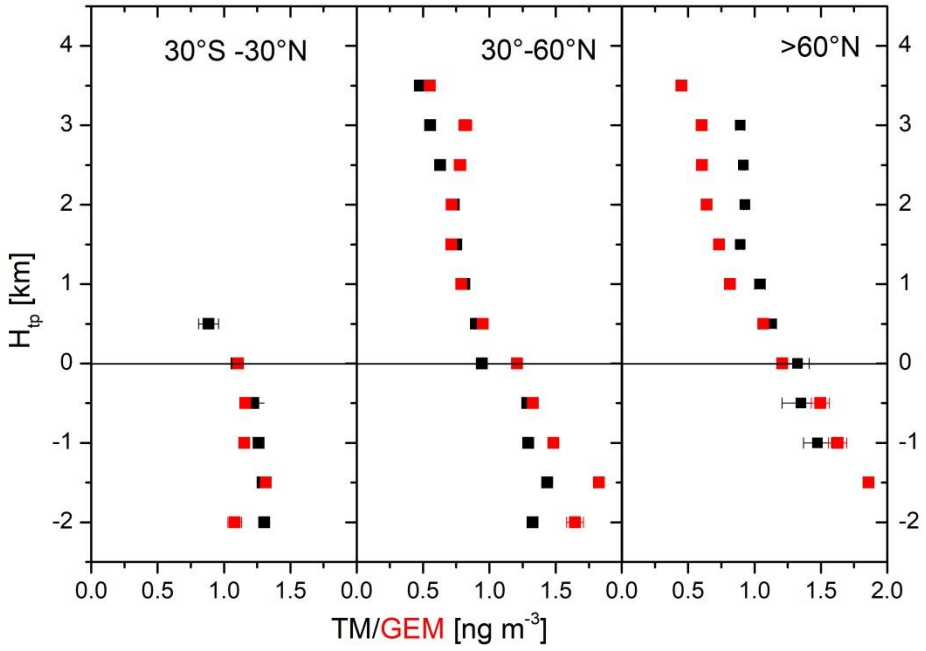

Figure 6: Stratospheric average TM and GEM concentrations in boreal winter (November – April) are binned according to the N_2O mixing ratio. N_2O mixing ratios were detrended using 2015 as a reference year and the N_2O growth rate of 0.844 ppb yr^{-1} (Assonov et al., 2013). Vertical and horizontal bars represent the standard errors of the averages.